Investigation of the Catalytic Mechanism of Sir2 Enzyme with QM/MM Approach: SN1 vs SN2?

Zhongjie Liang,[⊥,†] Ting Shi,[⊥,†] Sisheng Ouyang,[†] Honglin Li,[‡] Kunqian Yu,[†] Weiliang Zhu,[†,‡] Cheng Luo,[*,†,§] and Hualiang Jiang[*,†,‡]

Drug Discovery and Design Center, State Key Laboratory of Drug Research, Shanghai Institute of Materia Medica, Chinese Academy of Sciences, Shanghai 201203, China, School of Pharmacy, East China University of Science and Technology, Shanghai 200237, China, Center for Systems Biology, Soochow University, Jiangsu 215006, China

Received: June 13, 2010; Revised Manuscript Received: July 22, 2010

Sir2, the histone deacetylase III family, has been subjected to a wide range of studies because of their crucial roles in DNA repair, longevity, transcriptional silencing, genome stability, apoptosis, and fat mobilization. The enzyme binds NAD^+ and acetyllysine as substrates and generates lysine, 2′-*O*-acetyl-ADP-ribose, and nicotinamide as products. However, the mechanism of the first step in Sir2 deacetylation reaction from various studies is controversial. To characterize this catalytic mechanism of acetyllysine deacetylation by Sir2, we employed a combined computational approach to carry out molecular modeling, molecular dynamics (MD) simulations, quantum mechanics/molecular mechanics (QM/MM) calculations on catalysis by both yeast Hst2 (homologue of SIR two 2) and bacterial Sir2TM (Sir2 homologue from *Thermatoga maritima*). Our three-dimensional (3D) model of the complex is composed of Sir2 protein, NAD^+, and acetyllysine (ALY) substrate. A 15-ns MD simulation of the complex revealed that Gln115 and His135 play a determining role in deacetylation. These two residues can act as bases to facilitate the deprotonation of 2′-OH from *N*-ribose. The result is in great agreement with previous mutagenesis analysis data. QM/MM calculations were further performed to study the mechanism of the first step in deacetylation in the two systems. The predicted potential energy barriers for yHst2 and Sir2TM are 12.0 and 15.7 kcal/mol, respectively. The characteristics of the potential energy surface indicated this reaction belongs to a SN2-like mechanism. These results provide insights into the Sir2 mechanism of nicotinamide inhibition and have important implications for the discovery of effectors against Sir2 enzymes.

1. Introduction

The sirtuin (silent information regulator, Sir2) family of genes is a highly conserved group present in the genomes of organisms ranging from archaebacteria to eukaryotes.[1,2] These enzymes comprise an ancient family of NAD^+-dependent deacetylases and catalyze the deacetylation of a variety of proteins, including histones,[3,4] p53,[5,6] p300,[7] acetyl-CoA synthetase,[8] α-tubulin,[9] myoD, Foxo3,[10−12] Ku70, and NF-κB.[13] Their ability to deacetylate such a wide range of substrates has implicated the key role of the enzymes in a wide spectrum of biological functions,[14−16] including DNA repair and recombination, longevity, transcriptional silencing, genome stability, apoptosis, axonal protection, insulin signaling, and fat mobilization. In addition, hyperactivation of Sir2 enzymes has been shown to increase lifespan in yeast, worms, flies, and mice. Increased longevity is due to a Sir2-dependent, calorie-restricted diet in most of these animals,[17−19] and deletion or inhibition of Sir2 leads to short-lived species. The disorder of Sir2 activity in mammals has been implicated in diverse age-related diseases, including diabetes, obesity, and neurodegenerative disorders.[20,21]

The mechanism for Sir2 deacetylation has been extensively studied at both structural and enzymatic levels. Distinguished from the class I or II deacetylases that utilize a zinc catalytic site to hydrolyze acetyl substrate, class III deacetylase Sir2 is NAD^+ dependent. Structural and biochemical studies have revealed that the deacetylation of acetyl substrate is coupled to the hydrolysis of NAD^+ to nicotinamide and the unique metabolite 2′-*O*-acetyl-ADP-ribose (OAADPr), a potential second messenger.[22−24] Nicotinamide is the noncompetitive inhibitor due to the base exchange at the expense of deacetylation. The Sir2 enzymatic core is composed of a large Rossmann fold domain and a structurally more variable zinc-binding motif domain, and four loops connecting the two domains form a cleft in the central region of the core domain. The acetyllysine (ALY) and NAD^+ bind to the opposite sides of the cleft and highlight the region of the core domain containing the highest degree of sequence conservation within the Sir2 proteins, implying a conserved catalytic mechanism. Meanwhile, the NAD^+ can adopt multiconformations in different states of Sir2. In the absence of ALY peptide, the nicotinamide and *N*-ribose of NAD^+ adopt multiconformations in the Sir2 active site named nonproductive conformations. Upon binding ALY peptide, NAD^+ adopts a strained conformation as a productive conformation that buries the nicotinamide ring deep in a highly conserved pocket, called the C pocket.[25−27] In this state, the ALY is oriented to react with NAD^+.

Until now, mutagenesis studies and isotope labeling experiments have in principle elucidated the catalytic mechanism of Sir2 deacetylase, which is stated as follows: in the first step,

* Corresponding authors. Phone: 86-21- 50271399. Fax: +86-21-50807088. E-mails: (H.J.) hljiang@mail.shcnc.ac.cn, (C.L.) cluo@mail.shcnc.ac.cn.
† Shanghai Institute of Materia Medica.
‡ East China University of Science and Technology.
§ Soochow University.
⊥ These authors contributed equally to this work.

10.1021/jp1054183
Published on Web 08/20/2010

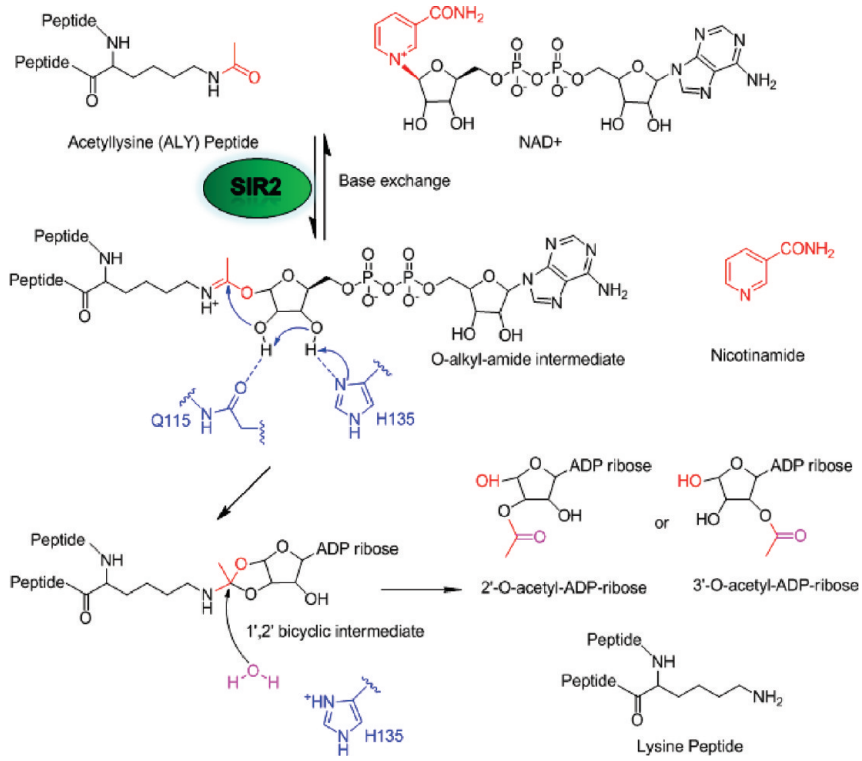

Figure 1. Proposed catalytic mechanism for Sir2.

the C1′ of the nicotinamide ribose (*N*-ribose) of NAD^+ is attacked by the nucleophilic carbonyl oxygen of ALY, which results in the cleavage of the nicotinamide-ribosyl bond of NAD^+ to release nicotinamide and the formation of a positively charged 1′-*O*-alkylamidate intermediate adduct between the two substrates;[28,29] in the subsequent step, 2′ OH of *N*-ribose is activated by the key surrounding amino acids, which leads to nucleophilic attack at the intermediate and generation of a 1′,2′-bicyclic species. Then a water attack on the cyclic intermediate and general acid-catalyzed elimination of the ε-amine of ALY yields the final two products OAADPr and deacetylated peptide.[30] The whole reaction process is shown in Figure 1. However, there have been two different structure-based mechanisms for the first step reaction, which concerns the breaking of the glycosidic bond and the transfer of the acetyl group. A dissociative, SN1-like mechanism was proposed on the basis of the structure of the yHst2 in complex with the acetylated histone H4 peptide and carba-NAD^+, a NAD^+ analogue in which the *N*-ribose oxygen is replaced by carbon.[25] Differently, associative a SN2-like mechanism was proposed on the basis of the structure of bacterial Sir2TM.[26]

Here, we report a study of the catalytic mechanism of Sir2 by combining molecular modeling, molecular dynamics (MD) simulations, and quantum mechanics/molecular mechanics (QM/MM) calculations. The molecular structure of the yHst2−ALY−NAD^+ complex in aqueous solution was obtained from the MD simulation. The simulation results reveal that Gln115 and His135 may play an essential role in both the *N*-ribose position and the deacetylation progress, which are in good agreement with the recent findings of mutagenesis experiments and related kinetic studies. On the basis of these results, we proposed a catalytic mechanism of this model enzyme for deacetylation using QM/MM calculations, which indicated the first step likely belongs to the SN2 mechanism. Consistently, the same result was obtained from the Sir2TM−ALY−NAD^+ complex model. Findings from this study provide a better understanding of the enzymatic mechanism of Sir2 and a potential explanation for the reduced enzyme activity caused by Sir2 mutations.

2. Materials and Methods

Molecular Modeling. Compared with the conformation of NAD^+ in Sir2TM−ALY−NAD^+ crystal structure (PDB code: 2H4F),[31] the carba-NAD in the yHst2−ALY−carba-NAD crystal structure (PDB code: 1SZC)[25] is in a different orientation. To obtain areasonable NAD^+ conformation and model the yHst2−ALY−NAD^+ complex, the Sir2TM−ALY−NAD^+ crystal structure was aligned with the yHst2−ALY−carba-NAD crystal structure by structural homology. Then the carba-NAD was replaced with NAD^+, which was extracted from the Sir2TM−ALY−NAD^+ structure. The initial yHst2−ALY−NAD^+ complex structure was minimized by using the AMBER force field with the following parameters: a distance-dependent dielectric function, nonbonded cutoff of 8 Å, Amber charges for the protein, and Gastieger−Hückel charges for ALY and NAD^+. The structure was minimized by the simplex method first, followed by the Powell method to an energy gradient <0.05 kcal/(mol·Å). All procedures were performed in the Sybyl software package (Tripos, St. Louis, MO).

The missing residues in the loop segment numbered from 37 to 42 (Asn37-GLy38-Ile39-Tyr40-Lys41-Lys42) in the Sir2TM−ALY−NAD^+ crystal structure were modeled by using the loop search method in the homology module of Insight 2005 (Accelrys, San Diego, CA). Finally, the complete complex structure was optimized by the aforementioned method.

Molecular Dynamics Simulation. MD simulations were performed on the yHst2−ALY−NAD^+ complex structure. Before simulations, the complex was put into a suitably sized box, of which the minimal distance from the protein to the box wall was 10 Å. Then the box was solvated with the SPC (simple point charge) water model. Then the complex water system was submitted to energy minimization. Afterward, counterions were

added to the system to provide a neutral simulation system. The whole system was subsequently minimized again. The charges of the atoms of NAD^+ and ALY were calculated by using the RESP method encoded in the AMBER suite of programs[32] at the level of RHF/6-31G*. Covalent and nonbonded parameters for the ligands atoms were assigned, by analogy or through interpolation, from those already present in the AMBER force field.

MD simulations were carried out using the AMBER package (version 10.0) with constant temperature and pressure (NPT) and periodic boundary conditions. The AMBER Parm99 force field was applied for the proteins. The particle mesh Ewald method was used to calculate the long-range electrostatics interactions. The nonbonded cutoff was set to 10.0 Å, and the nonbonded pairs were updated every 25 steps. The SHAKE method was applied to constrain all covalent bonds involving hydrogen atoms. Each simulation was coupled to a 300 K thermal bath at 1.0 atm of pressure (atm = 101.3 kPa) by applying the algorithm of Berendsen et al. The temperature and pressure coupling parameters were set as 1 ps. An integration step of 2 fs was set up for the MD simulations.

QM/MM Calculation. QM/MM calculations were performed by using a two-layered ONIOM method encoded in the Gaussian03 program.[33] The ONIOM method is a hybrid computational method developed by Morokuma and co-workers that allows different levels of theory to be applied to different parts of a molecular system.[34−42] In the two-layered ONIOM method, the molecular system under study is divided into an inner layer and an outer layer. The inner layer consists of the most critical elements of the system, and the rest of the system comprises the outer layer. In the terminology of Morokuma and co-workers, the full system is called "real" and is treated with a low level of theory. The inner layer is termed "model" and is treated with both the low level of theory and a high level of theory. The total ONIOM energy, E_{ONIOM}, is given as the following,

$$E_{\mathrm{ONIOM}} = E(\text{high, model}) + E(\text{low, real}) - \mathrm{E}(\text{low, model})$$

where E(high, model) is the energy of the inner layer (plus the link atoms) at the high level of theory, and E(low, real) is the energy of the entire system at the low level of theory. Thus, the ONIOM method allows one to perform a high-level calculation on just a small, critical part of the molecular system and incorporate the effects of the surrounding elements at a lower level of theory to yield a consistent energy expression on the full system.

The minimized yHst2−ALY−NAD^+ complex structure optimized using the AMBER Parm99 force field was further optimized at the ONIOM (B3LYP/6-31G*:AMBER) level. The quantum mechanics (QM) region includes the nicotinamide and *N*-ribose of the NAD^+, the acetyl terminal ($-CH_2-NHCOCH_3$) of acetyllysine, the backbone (−CH−CO−NH) of Gln115, and the side chain ($-CH_2-C_3N_2H_3$) of His135, for a total of 56 atoms. The QM region was calculated by using the density functional theory with the B3LYP exchange-correlation functional and 6-31G* basis set. The remainder of the system (MM region) was treated by using the AMBER Parm99 force field. A total of 4895 atoms in the system were included for the QM/MM simulations by using the ONIOM module as implemented in Gaussian 03. The electrostatic interactions between the QM and MM regions were calculated by using the electronic embedding method, which treats the polarization of the QM region by the MM region with scaled partial atomic charges of MM atoms and the response of the QM region with the Merz−Singh−Kollman scheme for charge fitting so as to produce the changing partial charges of the QM atoms. The same procedure was processed on the Sir2TM−ALY−NAD^+ complex structure system, and a total of 4168 atoms were included for the QM/MM calculations by using the ONIOM module in Gaussian 03.

3. Results and Discussion

The main goal of this study is to investigate the catalytic process of Sir2 by using computational methods. Such a study, however, needs an accurate structural model for the whole catalytic environment of Sir2 with NAD^+ and ALY peptide. Accordingly, a 3D model of the Sir2 complex, yHst2−ALY−NAD^+, was constructed on the basis of the high-resolution structure of yeast Hst2 (homologue of SIR two 2, PDB ID code: 1SZC)[25] with an acetyllysine histone H4 peptide and carba-NAD^+. Then the dynamic conformational change of the catalytic site of this model was investigated by performing MD simulations. Furthermore, the simulation results were validated by previous mutagenesis and enzymatic kinetic assays. Encouraged by the compatible results from MD simulations and relevant experiments, we further explored the catalytic mechanism of the yHst2−ALY−NAD^+ system for the first step in deacetylation by using QM/MM calculations. In addition, we performed QM/MM calculations on the modeled bacterial Sir2TM complex (PDB ID code: 2H4F)[31] with the acetylated peptide p53 and NAD^+, Sir2TM−ALY−NAD^+, to reinforce our conclusion.

MD Simulation Was Reasonable on yHst2−ALY−NAD^+ System. To study the stability of the reaction environment, a 15-ns MD simulation was performed on the yHst2−ALY−NAD^+ complex. The time evolutions of the root-mean-square deviations (RMSD) for the atoms of yHst2 from their initial positions (t = 0 ps) were monitored. The result indicates that the catalytic environment of yHst2 is relatively stable during the simulation. Meanwhile, the root-mean-square fluctuations (RMSF), which represents average displacement of residues along the whole simulation process, reflects that the $\beta1-\alpha2$ loop (residues 35−63), zinc-binding loops, and terminal loops of yHst2 are more flexible, as shown in Figure 2. The $\beta1-\alpha2$ loop of Sir2 proteins harbors a high degree of sequence conservation, indicating its functional importance, yet the comparison of yHst2 structures with NAD^+ substrate in different states shows the greatest structural variability in the $\beta1-\alpha2$ loop. It was indicated that the relatively open conformation of this loop facilitates NAD^+ substrate access, and the closed conformation plays a key role in nicotinamide release.[25] Consequently, the consistency between the theoretical RMSF value and the experimental B factor value signifies that the MD simulation on yHst2−ALY−NAD^+ system is reasonable.

Key Residues H-Bond with NAD^+ in the Catalytic Site in MD Simulation. The H-bond network in yHst2−ALY−NAD^+ complex reflects the stability of the deacetylation environment and indicates some key residues in the catalytic process. These H-bonds were mostly maintained during the MD simulation, as shown in Figure 3. In the conserved C pocket, the NH group of Ile117 and the atom $O^{\gamma1}$ of the Asp118 H-bond with the amide group of the nicotinamide moiety of NAD^+, which makes the NAD^+ accessible to the productive conformation. The *N*-ribose of NAD^+, which was considered flexible in the catalytic process,[25,43] is stabilized by the H-bonds, involving the O atom of Gln115 and the N^{δ} atom of His135 with the 2′ and 3′ OH of the *N*-ribose, respectively.

Meanwhile, the carbonyl oxygen of ALY can H-bond with the 2′ and 3′ OH of *N*-ribose. These may be another key factor

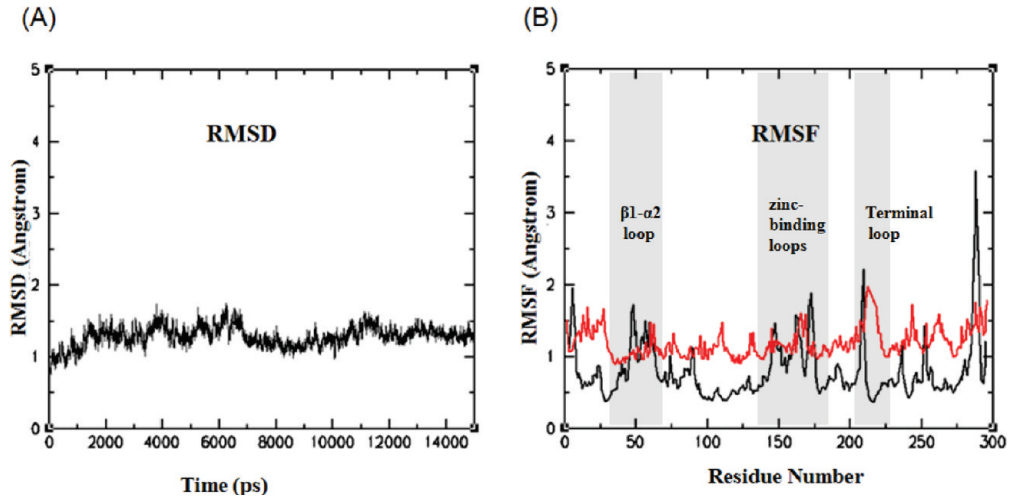

Figure 2. (A) Time dependencies of the weighted root-mean-square deviations (wRMSDs) for the backbone atoms of yHst2 from their initial positions during the 15-ns simulation. (B) Residue fluctuations obtained by averaging residual fluctuations over the MD simulation (black curve) and by computing the value from experimentally derived B factors (red curve) for the yHst2 crystal structure.

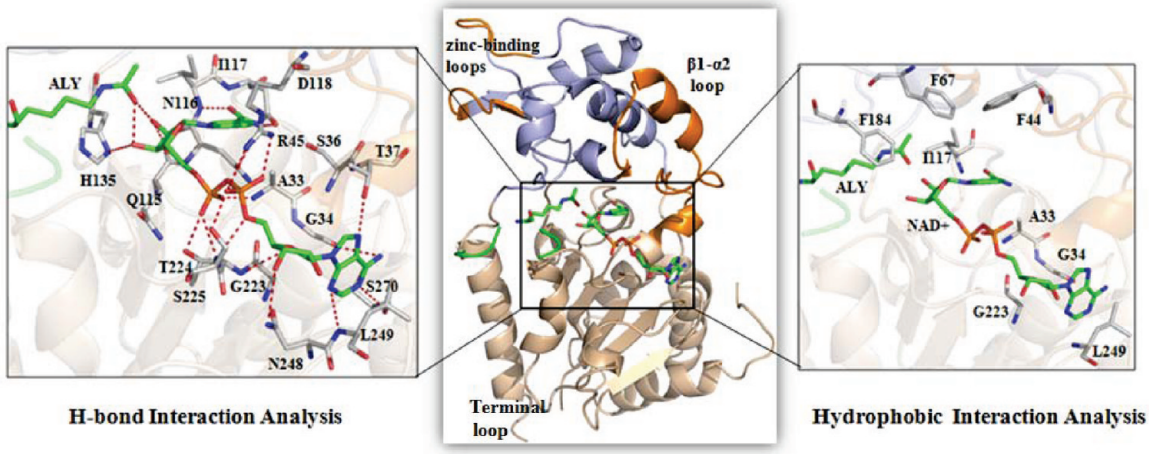

Figure 3. Overall structure of yHst2−ALY−NAD^+ complex and the interactions. Cartoon diagram of the yHst2−ALY−NAD^+ complex highlighting the large domain (light blue), small domain (wheat), zinc-binding loops and β1-α2 loop (orange), and ALY peptide and NAD^+ (green). H-bond interaction indicates the yHst2 residues (carbon, white; oxygen, red; and nitrogen, blue) that hydrogen bond with NAD^+. H-bonds are indicated with red dashed lines. Meanwhile, hydrophobic interaction indicates the yHst2 residues forming hydrophobic interactions with NAD^+.

for NAD^+ productive conformation. As for the ADP part of NAD^+, a stable H-bond network is formed with the conserved residues (e.g. Ala33, Gly34, Thr37, Arg45, Thr224, Ser225, Asn248, and Ser270), which are conserved in the Sir2 family. Among all these conserved residues H-bonding with NAD^+, their key roles have been validated by the mutagenesis experiments, especially for the residues H-bonding with nicotinamide and *N*-ribose. For instance, Ile117, and Asp118 mutant experiments have revealed their dominant roles in nicotinamide release and inhibition activity due to their H-bonds or volume occupancy.[27,44]

Mutation of this His135 in sirtuin homologues leads to decreased enzymatic turnover in vitro and loss of transcriptional silencing in vivo.[45,46] This is because after the attack of the carbonyl oxygen of ALY on the C1′ carbon on the α face of the *N*-ribose and the release of the nicotinamide, the residue can act as the base to activate the 2′ hydroxy oxygen to facilitate the follow-up reactions. However, it is proved that the deacetylation reaction is not only dependent on contacts with His135.[45] Nevertheless, this is consistent with our results that Gln115 is another key factor in binding and positioning NAD^+ into its productive conformation. In addition, this crucial role of Gln115 is also quite in agreement with the fact that the base exchange and deacetylase activities are significantly reduced when this residue is mutated to alanine in *Archaeoglobus fulgidus*.[46]

Together, both Gln115 and His135 are considered to be the crucial factor for positioning the *N*-ribose and activating the hydroxyl groups of *N*-ribose. Overall, under the restriction of all these key residues, ALY and NAD^+ form a highly advantageous configuration for the biochemical reaction. The ALY carbonyl is within 3.39 Å of the C1′ position and is in the proper orientation for nucleophilic attack.

Key Residues Form Hydrophobic Interactions with NAD^+. As for the hydrophobic interactions, contacts with Phe44, Phe67, and Phe184 help bury the nicotinamide ring in a largely hydrophobic environment within the C pocket. Among these residues, the phenylalanines may be positioned to protect the 1′-*O*-alkylamidate intermediate from base exchange with nicotinamide or solvent hydrolysis, and they are mostly located above the *N*-ribose and nicotinamide during the MD simulation, despite the flexible β1−α2 loop, shown in Figure 3. The Sir2TM F33A mutant is more accessible to nicotinamde inhibition, and the deacetylation reactions decreases significantly.[43] Meanwhile, the invariant Gly38-Ala39-Gly40 motif in the β1−α2 loop that is a little distant from the nicotinamide in this open conformation may be another favorable factor for the hydrophobic environ-

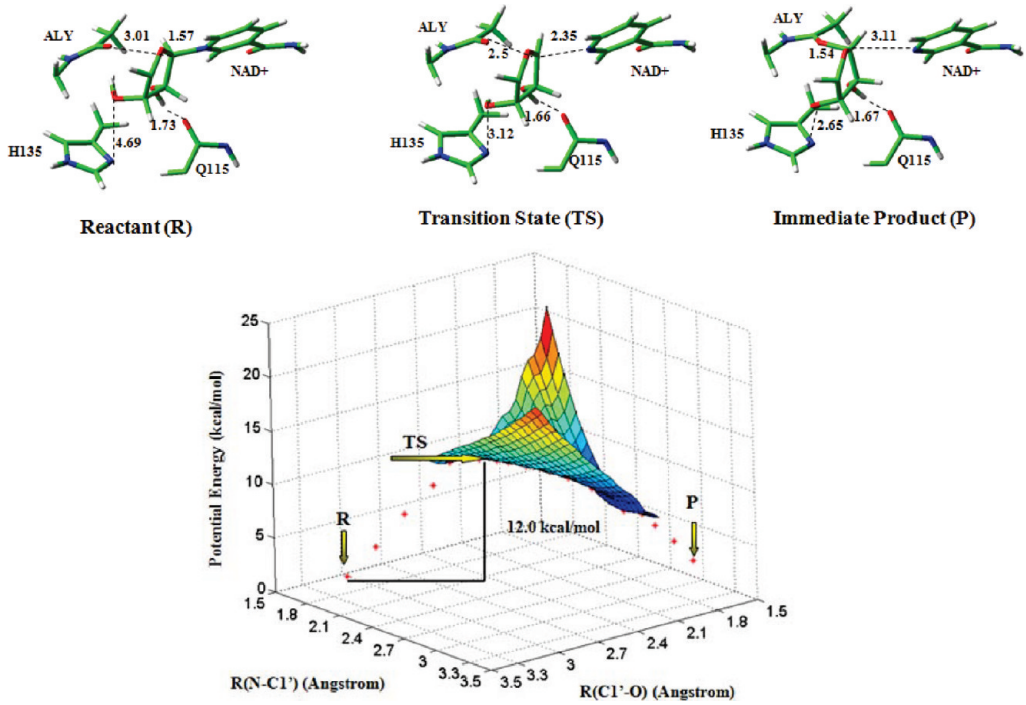

Figure 4. The potential energy surface of the reaction pathway corresponding to the first step in the deacetylation of yHst2−ALY−NAD^+ complex. The structures displayed at the top of the potential surface are the QM/MM optimized structures of the reactant (R), transition state (TS), and immediate product (P). For clarity, only the structures in the QM region have been shown.

ment of the C pocket. In addition, other residues forming hydrophobic interactions with ADP ribose, as shown in Figure 3, are almost conserved in Sir2 homologues.

QM/MM Results. To further explore the detailed mechanism of the first step in the deacetylation reaction, the QM/MM approach was performed on the yHst2−ALY−NAD^+ complex. From the RMSD analysis in MD simulation shown in Figure 2A, the system begins to reach equilibrium from 2 ns. Within the trajectory, the middle point in the equilibrium state (t = 8 ns) was located to be the most flat curve and then extracted for exploring the possibility to be the starting point for further QM/MM study. As shown in Figure 3, the interaction analysis based on the snapshot indicates the surrounding residues forming H-bonds and hydrophobic interactions with NAD^+ in the complex were quite compatible with the previous experimental studies,[27,43−46] which confirmed the snapshot was a good starting point for the QM/MM study.

In the QM/MM simulation, the QM region was composed not only of nicotinamide and *N*-ribose of NAD^+ and the terminal acetyl group of acetyllysine but also of the backbone of Gln115 and side chain of His135, considering the key roles of Gln115 and His135 in deacetylation. The remainder of the complex was included in the MM region. The partitioning scheme for QM and MM regions is described in the Materials and Methods section. We designate this structure as a reactant system. ONIOM (our own *N*-layer integrated molecular orbital molecular mechanics), a QM/MM method encoded in Gaussion03, was performed for all the QM/MM calculations.

When comparing the initial structure obtained by MD simulation with the QM/MM optimized structure, the main difference of the reaction center is that the N−C1′ distance is elongated from 1.48 to 1.57 Å. The trend indicated that the nicotinamide release possesses a partial dissociative mechanism feature. Then we propose a mechanism for the first step in deacetylation catalyzed by yHst2, as shown in Figure 4. Along this reaction path, the energies of the reactant (R), transition state (TS), and immediate product (P) were determined by two-dimensional QM/MM potential energy surface by defining the distances of R(N−C1′) and R(C1′−O) as the reaction coordinates. In the optimized reactant, R(N−C1′) = 1.57 Å and R(C1′−O) = 3.01 Å; and in the optimized immediate product, the N−C1′ bond is broken, and the C1′−O is formed (R(C1′−O) = 1.54 Å).

A potential energy barrier of 12.0 kcal/mol was required for the *O*-alkyl-amide immediate formation. The structure of the transition state (TS) was determined by adiabatic mapping at the QM/MM level, in the TS, R(N−C1′) = 2.35 Å and R(C1′−O) = 2.5 Å, which are much longer than their covalent bond distances. Thus, the TS for this nicotinamide cleavage reaction can be considered very loose and highly dissociative. The H1 is turned to be in a plane with the *N*-ribose ring in the TS, and the structure illustrates that the N−C1′ bond is partially broken and the C1′−O bond is partially formed. This result indicates that the first step belongs to the SN2 mechanism, and the overall reaction is calculated to be endothermic by ΔE = 2.65 kcal/mol. Furthermore, to investigate the conformational change of the catalytic region along the SN1 mechanism, the N−C1′ bond was constrained and elongated from 1.6 to 3.0 Å, and the full optimization was performed for the remainder. Unfortunately, the immediate product of NAD^+ with nicotinamide cleavage, supposed as the symbol of the SN1 mechanism, was not obtained with our careful calculation. As the distance between the N and C1′ elongates, the O of the acetyl group draws closer to the C1′ automatically until it reaches an immediate product, which was consistent with that obtained by the SN2 mechanism. The result definitely indicates the reaction belongs to the SN2 mechanism. Along the reaction pathway, the TS state was located as R(N−C1′) = 2.30 Å and R(C1′−O) = 2.42 Å, and the potential energy barrier was about 11.7 kcal/mol. The corresponding figure is shown in the Support Information.

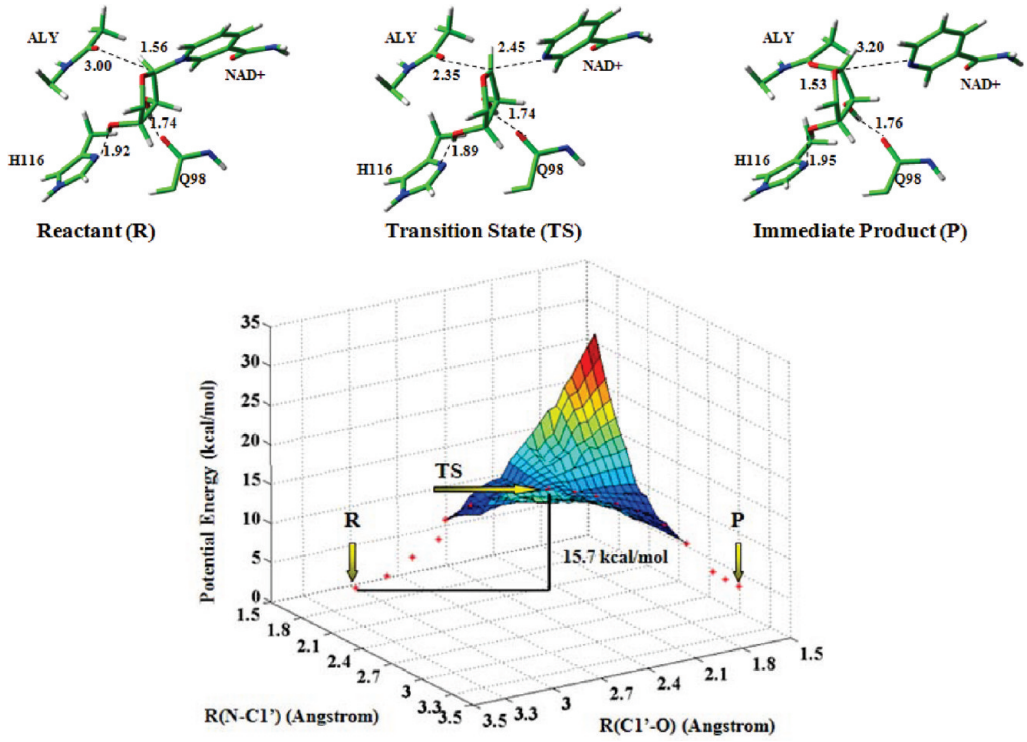

Figure 5. The potential energy surface of the reaction pathway corresponding to the first step in the deacetylation of Sir2TM−ALY−NAD^+ complex. The structures displayed at the top of the potential surface are the QM/MM optimized structures of the reactant (R), transition state (TS), and immediate product (P). For clarity, only the structures in the QM region have been shown.

To further validate this conclusion, we investigated the bacterial Sir2TM with acetylated peptide p53 and NAD^+, Sir2TM−ALY−NAD^+, by employing the same QM/MM method. The major difference between the optimized structure of the Sir2TM system and yHst2 system is that an intermolecular H-bond in the former system was replaced by another intramolecular H-bond in the latter. In detail, the H-bond was formed between the 3′ O and N of His116 in the Sir2TM−ALY−NAD^+ system, but it was changed into the H-bond between the 2′ O and 3′ O of the *N*-ribose in the yHst2−ALY−NAD^+ system. In the Sir2TM reaction center, the N^{δ} atom of His116 and the O atom of Q98 can form strong H-bonds with the 2′ OH and 3′ OH of the *N*-ribose, respectively, which may contribute to the arrangement of NAD^+ and activate the 2′ O of *N*-ribose. In other words, His116 and Q98 can be used as bases to facilitate the following reaction.

As shown in Figure 5, in the optimized reactant, R(N−C1′) = 1.56 Å and R(C1′−O) = 3.00 Å, similar to the yHst2 complex reactant, and in the optimized immediate product, the N−C1′ bond is broken and the C1′−O bond is formed, R(C1′−O) = 1.53 Å. A potential energy barrier of 15.7 kcal/mol was required for the 1′-*O*-alkylamide immediate formation. The structure of the transition state (TS) was determined by adiabatic mapping at the QM/MM level, in the TS, R(N−C1′) = 2.45 Å and R(C1′−O) = 2.35 Å, and the H1 is turned to be in a plane with the *N*-ribose ring. This structure illustrates that the N−C1′ bond is partially broken and the C1′−O bond is partially formed, which is consistent with the result of the yHst2 complex system. This result again proved that the first step belongs to SN2 mechanism, and the overall reaction is calculated to be endothermic by ΔE = 4.98 kcal/mol.

4. Conclusions

As mentioned above, Sir2 plays a crucial role in DNA repair, longevity, transcriptional silencing, genome stability, apoptosis, and fat mobilization. However, the mechanism of Sir2 deacetylation reaction remains unclear, and especially, a heated controversy still lies in the first step of this reaction. Therefore, in this study, we focused on the first step of the deacetylation reaction in the yHst2 (and Sir2TM)−ALY−NAD^+ system and theoretically confirmed that the first step of this deacetylation reaction belongs to the SN2 mechanism, which agrees well with Po Hu's study.[47] First, we employed MD simulation on the yHst2−ALY−NAD^+ complex and got a stable structure on the snapshot at 8000 ps of the MD trajectory. The validity of the MD simulation was confirmed by the agreement between the available experimental mutagenesis and enzymatic data for Sir2 homologues and the important interactions of yHst2 with NAD^+. Among the residues forming H-bonds or hydrophobic interactions with NAD^+, Gln115 and His135 were considered to play key roles in positioning the NAD^+ and act as a general base catalyst to activate 2′ or 3′ OH deprotonation for catalysis. Second, the QM/MM calculations were performed on the stable yHst2 complex system, and in addition to the groups participating in the reaction, the backbone of Gln115 and the side chain of His135 were selected in the QM region, too. Although the transition state is very loose and indicates the nicotinamide cleavage reaction possesses a highly dissociative feature, the two-dimensional QM/MM potential energy surface proved that the reaction basically belongs to the SN2 mechanism. To further validate this result, we performed QM/MM calculations again on bacterial Sir2TM, and the same conclusion was obtained. Our research thus provided a detailed mechanism for the first step of deacetylation by Sir2 proteins, explored a molecular basis for this reaction, and lighted up the road for further discovery of modular effectors of Sir2.

Acknowledgment. We gratefully thank Dr. Marmorstein for his helpful comments. We also gratefully acknowledge financial support from the National Natural Science Foundation of China

(20720102040, 20803022, and 20972174), the Hi-Tech Research and Development Program of China (2006AA01A124), the State Key Program of Basic Research of China Grant (2009CB918502 and 2009CB940901), Shanghai Committee of Science and Technology Grant (10410703900), and National S&T Major Project (2009ZX09501-001), Information Construction Project of the Chinese Academy of Sciences (no. INFO-115-B01), State Key Laboratory Grant (SIMM1004KF-15) and Guangdong Science and Technology Department (2010A030100006).

Supporting Information Available: Additional information as noted in the text. This material is available free of charge via the Internet at http://pubs.acs.org.

References and Notes

(1) Frye, R. A. *Biochem. Biophys. Res. Commun.* **1999**, *260*, 273.
(2) Frye, R. A. *Biochem. Biophys. Res. Commun.* **2000**, *273*, 793.
(3) Chang, K. T.; Min, K. T. *Ageing Res. Rev.* **2002**, *1*, 313.
(4) Shankaranarayana, G. D.; Motamedi, M. R.; Moazed, D.; Grewal, S. I. *Curr. Biol.* **2003**, *13*, 1240.
(5) Avalos, J. L.; Celic, I.; Muhammad, S.; Cosgrove, M. S.; Boeke, J. D.; Wolberger, C. *Mol. Cell* **2002**, *10*, 523.
(6) Tikoo, K.; Tripathi, D. N.; Kabra, D. G.; Sharma, V.; Gaikwad, A. B. *FEBS Lett.* **2007**, *581*, 1071.
(7) Han, Y.; Jin, Y. H.; Kim, Y. J.; Kang, B. Y.; Choi, H. J.; Kim, D. W.; Yeo, C. Y.; Lee, K. Y. *Biochem. Biophys. Res. Commun.* **2008**, *375*, 576.
(8) Starai, V. J.; Takahashi, H.; Boeke, J. D.; Escalante-Semerena, J. C. *Curr. Opin. Microbiol.* **2004**, *7*, 115.
(9) North, B. J.; Marshall, B. L.; Borra, M. T.; Denu, J. M.; Verdin, E. *Mol. Cell* **2003**, *11*, 437.
(10) Brunet, A.; Sweeney, L. B.; Sturgill, J. F.; Chua, K. F.; Greer, P. L.; Lin, Y.; Tran, H.; Ross, S. E.; Mostoslavsky, R.; Cohen, H. Y.; Hu, L. S.; Cheng, H. L.; Jedrychowski, M. P.; Gygi, S. P.; Sinclair, D. A.; Alt, F. W.; Greenberg, M. E. *Science* **2004**, *303*, 2011.
(11) Motta, M. C.; Divecha, N.; Lemieux, M.; Kamel, C.; Chen, D.; Gu, W.; Bultsma, Y.; McBurney, M.; Guarente, L. *Cell* **2004**, *116*, 551.
(12) Daitoku, H.; Hatta, M.; Matsuzaki, H.; Aratani, S.; Ohshima, T.; Miyagishi, M.; Nakajima, T.; Fukamizu, A. *Proc. Natl. Acad. Sci. U.S.A.* **2004**, *101*, 10042.
(13) Kawahara, T. L.; Michishita, E.; Adler, A. S.; Damian, M.; Berber, E.; Lin, M.; McCord, R. A.; Ongaigui, K. C.; Boxer, L. D.; Chang, H. Y.; Chua, K. F. *Cell* **2009**, *136*, 62.
(14) Smith, J. S.; Avalos, J.; Celic, I.; Muhammad, S.; Wolberger, C.; Boeke, J. D. *Methods Enzymol.* **2002**, *353*, 282.
(15) Blander, G.; Guarente, L. *Annu. Rev. Biochem.* **2004**, *73*, 417.
(16) Chakrabarty, S. P.; Saikumari, Y. K.; Bopanna, M. P.; Balaram, H. *Mol. Biochem. Parasitol.* **2008**, *158*, 139.
(17) Cohen, H. Y.; Miller, C.; Bitterman, K. J.; Wall, N. R.; Hekking, B.; Kessler, B.; Howitz, K. T.; Gorospe, M.; de Cabo, R.; Sinclair, D. A. *Science* **2004**, *305*, 390.
(18) Kaeberlein, M.; Hu, D.; Kerr, E. O.; Tsuchiya, M.; Westman, E. A.; Dang, N.; Fields, S.; Kennedy, B. K. *PLoS Genet.* **2005**, *1*, e69.
(19) Lin, S. J.; Guarente, L. *PLoS Genet.* **2006**, *2*, e33; author reply e34.
(20) Guarente, L.; Picard, F. *Cell* **2005**, *120*, 473.
(21) Mostoslavsky, R.; Chua, K. F.; Lombard, D. B.; Pang, W. W.; Fischer, M. R.; Gellon, L.; Liu, P.; Mostoslavsky, G.; Franco, S.; Murphy, M. M.; Mills, K. D.; Patel, P.; Hsu, J. T.; Hong, A. L.; Ford, E.; Cheng, H. L.; Kennedy, C.; Nunez, N.; Bronson, R.; Frendewey, D.; Auerbach, W.; Valenzuela, D.; Karow, M.; Hottiger, M. O.; Hursting, S.; Barrett, J. C.; Guarente, L.; Mulligan, R.; Demple, B.; Yancopoulos, G. D.; Alt, F. W. *Cell* **2006**, *124*, 315.
(22) Tanner, K. G.; Landry, J.; Sternglanz, R.; Denu, J. M. *Proc. Natl. Acad. Sci. U.S.A.* **2000**, *97*, 14178.
(23) Tanny, J. C.; Moazed, D. *Proc. Natl. Acad. Sci. U.S.A.* **2001**, *98*, 415.
(24) Sauve, A. A.; Celic, I.; Avalos, J.; Deng, H.; Boeke, J. D.; Schramm, V. L. *Biochemistry* **2001**, *40*, 15456.
(25) Zhao, K.; Harshaw, R.; Chai, X.; Marmorstein, R. *Proc. Natl. Acad. Sci. U.S.A.* **2004**, *101*, 8563.
(26) Avalos, J. L.; Boeke, J. D.; Wolberger, C. *Mol. Cell* **2004**, *13*, 639.
(27) Avalos, J. L.; Bever, K. M.; Wolberger, C. *Mol. Cell* **2005**, *17*, 855.
(28) Denu, J. M. *Trends Biochem. Sci.* **2003**, *28*, 41.
(29) Sauve, A. A.; Schramm, V. L. *Curr. Med. Chem.* **2004**, *11*, 807.
(30) Borra, M. T.; Langer, M. R.; Slama, J. T.; Denu, J. M. *Biochemistry* **2004**, *43*, 9877.
(31) Zhang, J.; Li, C.; Shi, T.; Chen, K.; Shen, X.; Jiang, H. *PLoS One* **2009**, *4*, e6304.
(32) Case, D. A.; Cheatham, T. E., 3rd; Darden, T.; Gohlke, H.; Luo, R.; Merz, K. M., Jr.; Onufriev, A.; Simmerling, C.; Wang, B.; Woods, R. J. *J. Comput. Chem.* **2005**, *26*, 1668.
(33) Akritopoulou-Zanze, I.; Hajduk, P. J. *Drug Discovery Today* **2009**, *14*, 291.
(34) Albrecht, B. K.; Harmange, J. C.; Bauer, D.; Berry, L.; Bode, C.; Boezio, A. A.; Chen, A.; Choquette, D.; Dussault, I.; Fridrich, C.; Hirai, S.; Hoffman, D.; Larrow, J. F.; Kaplan-Lefko, P.; Lin, J.; Lohman, J.; Long, A. M.; Moriguchi, J.; O'Connor, A.; Potashman, M. H.; Reese, M.; Rex, K.; Siegmund, A.; Shah, K.; Shimanovich, R.; Springer, S. K.; Teffera, Y.; Yang, Y.; Zhang, Y.; Bellon, S. F. *J. Med. Chem.* **2008**, *51*, 2879.
(35) Bellon, S. F.; Kaplan-Lefko, P.; Yang, Y.; Zhang, Y.; Moriguchi, J.; Rex, K.; Johnson, C. W.; Rose, P. E.; Long, A. M.; O'Connor, A. B.; Gu, Y.; Coxon, A.; Kim, T. S.; Tasker, A.; Burgess, T. L.; Dussault, I. *J. Biol. Chem.* **2008**, *283*, 2675.
(36) Bogoyevitch, M. A.; Fairlie, D. P. *Drug Discovery Today* **2007**, *12*, 622.
(37) Cai, Z. W.; Wei, D.; Schroeder, G. M.; Cornelius, L. A.; Kim, K.; Chen, X. T.; Schmidt, R. J.; Williams, D. K.; Tokarski, J. S.; An, Y.; Sack, J. S.; Manne, V.; Kamath, A.; Zhang, Y.; Marathe, P.; Hunt, J. T.; Lombardo, L. J.; Fargnoli, J.; Borzilleri, R. M. *Bioorg. Med. Chem. Lett.* **2008**, *18*, 3224.
(38) Chen, L.; Li, H.; Liu, J.; Zhang, L.; Liu, H.; Jiang, H. *Bioorg. Med. Chem.* **2007**, *15*, 6763.
(39) D'Angelo, N. D.; Bellon, S. F.; Booker, S. K.; Cheng, Y.; Coxon, A.; Dominguez, C.; Fellows, I.; Hoffman, D.; Hungate, R.; Kaplan-Lefko, P.; Lee, M. R.; Li, C.; Liu, L.; Rainbeau, E.; Reider, P. J.; Rex, K.; Siegmund, A.; Sun, Y.; Tasker, A. S.; Xi, N.; Xu, S.; Yang, Y.; Zhang, Y.; Burgess, T. L.; Dussault, I.; Kim, T. S. *J. Med. Chem.* **2008**, *51*, 5766.
(40) Ghose, A. K.; Herbertz, T.; Pippin, D. A.; Salvino, J. M.; Mallamo, J. P. *J. Med. Chem.* **2008**, *51*, 5149.
(41) He, L.; Zhang, L.; Liu, X.; Li, X.; Zheng, M.; Li, H.; Yu, K.; Chen, K.; Shen, X.; Jiang, H.; Liu, H. *J. Med. Chem.* **2009**, *52*, 2465.
(42) Kim, K. S.; Zhang, L.; Schmidt, R.; Cai, Z. W.; Wei, D.; Williams, D. K.; Lombardo, L. J.; Trainor, G. L.; Xie, D.; Zhang, Y.; An, Y.; Sack, J. S.; Tokarski, J. S.; Darienzo, C.; Kamath, A.; Marathe, P.; Lippy, J.; Jeyaseelan, R., Sr.; Wautlet, B.; Henley, B.; Gullo-Brown, J.; Manne, V.; Hunt, J. T.; Fargnoli, J.; Borzilleri, R. M. *J. Med. Chem.* **2008**, *51*, 5330.
(43) Hawse, W. F.; Hoff, K. G.; Fatkins, D. G.; Daines, A.; Zubkova, O. V.; Schramm, V. L.; Zheng, W.; Wolberger, C. *Structure* **2008**, *16*, 1368.
(44) Sanders, B. D.; Zhao, K.; Slama, J. T.; Marmorstein, R. *Mol. Cell* **2007**, *25*, 463.
(45) Hoff, K. G.; Avalos, J. L.; Sens, K.; Wolberger, C. *Structure* **2006**, *14*, 1231.
(46) Min, J.; Landry, J.; Sternglanz, R.; Xu, R. M. *Cell* **2001**, *105*, 269.
(47) Hu, P.; Wang, S.; Zhang, Y. *J. Am. Chem. Soc.* **2008**, *130*, 16721.

JP1054183